catalysts

MDPI

Article

Synergistic Enhancement in Catalytic Performance of Superparamagnetic Fe_3O_4@*Bacilus subtilis* as Recyclable Fenton-Like Catalyst

Pei Zheng [1,*], Zhe Pan [2] and Jun Zhang [1,3]

1 College of Geography and Environment, Baoji University of Arts and Sciences, Baoji 721013, China; zhangjun1190@126.com

2 College of Chemistry and Chemical Engineering, Baoji University of Arts and Sciences, Baoji 721013, China; panzhe19880116@163.com

3 Key Laboratory of Subsurface Hydrology and Ecological Effects in Arid Region, Chang'an University, Xi'an 710064, China

* Correspondence: zhengpei19890220@163.com; Tel.: +86-159-0291-6848

Received: 27 August 2017; Accepted: 3 October 2017; Published: 20 November 2017

Abstract: Novel well-defined superparamagnetic Fe_3O_4@*Bacilus subtilis* composite (Fe_3O_4@*B. subtilis* SPMC) was synthesized through a facile electrostatic attraction method and used as a recyclable heterogeneous Fenton-like catalyst. With the presence of H_2O_2, Fe_3O_4@*B. subtilis* SPMC can remove nearly 87% of the doxycycline at the initial concentration of 50 mg L^{-1}, exhibiting enhanced Fenton-like catalytic performance than pristine Fe_3O_4. The mechanism study demonstrates the synergistic effect between *Bacilus subtilis* adsorption and Fenton-like ability of Fe_3O_4 dominates the enhancement for Fenton-like catalytic efficiency of Fe_3O_4@*B. subtilis* SPMC. The obtained composite shows excellent recycling ability, reusability, and stability, which pave a new way for future design on highly efficient Fenton-like catalyst for degradation of organic pollutants.

Keywords: Fe_3O_4; *Bacilus subtilis*; synergistic effect; Fenton-like; recyclable; superparamagnetic

1. Introduction

Magnetite (Fe_3O_4) has attracted growing research interests in various fields, such as Li ion batteries [1], catalysts [2], drug delivery and targeting [3], etc., due to its distinguished physical and chemical properties [4,5]. However, these magnetite Fe_3O_4 nanoparticles (MNPs) may aggregate into large clusters because of the anisotropic dipolar interactions, reducing their dispersibility and other specific properties and ultimately diminishing their activity [6]. In addition, another challenge that impedes the practical application of Fe_3O_4 is the production of iron-containing waste sludge, which introduces secondary pollution [7,8]. Hence, to overcome these disadvantages, significant efforts have been made to immobilize the Fe_3O_4 particles onto various support materials, simultaneously preserving their unique magnetic property [9–12].

Lately, microorganisms employed as support materials has being attracting great interest because of their major advantages such as ample resources, environmentally friendliness, and abundant functional groups [13]. *Bacillus subtilis* is a kind of genus *Bacillus* and can be easily found in water, soil, air, and decomposing plant matter [13–15]. Thus, owing to its distinguished physicochemical/biological properties, *B. subtilis* has been selected as an ideal candidate for the synthesis of composite materials for organic pollutants removal [13–16]. However, until now, no one has been focused on the preparation and application of integrated Fe_3O_4@*B. subtilis* heterogeneous catalyst.

In this study, we present a facile electrostatic attraction method for the coating of Fe_3O_4 nanoparticles onto the surfaces of *B. subtilis* to form superparomagnetic recyclable Fe_3O_4@*B. subtilis*

heterogeneous Fenton-like catalyst. The morphology, crystal structure, functional groups, magnetic property, and Fenton-like catalytic performance of Fe_3O_4@*B. subtilis* superparomagnetic composite (Fe_3O_4@*B. subtilis* SCP) are systematically characterized and evaluated. The catalytic performance of Fe_3O_4@*B. subtilis* SCP is significantly enhanced compared to the pristine Fe_3O_4. The prepared Fe_3O_4@*B. subtilis* SCP exhibits excellent recycling ability due to its superparamagnetic feature. The outstanding reusability was evaluated by successive batches of Doxycyline (DC) degradation, and the good chemical stability was also investigated by X-ray diffraction (XRD) and X-ray photoelectron spectroscopy (XPS). The leaching of iron ions from Fe_3O_4@*B. subtilis* was evaluated by inductively coupled plasma mass spectrometry (ICP-MS). The mechanism for the enhanced Fenton-like catalytic activity of Fe_3O_4@*B. subtilis* SCP is proposed and investigated through photoluminescence (PL) study.

2. Results and Discussion

2.1. Characterization

The pristine *B. subtilis* cells (Figure 1a) are rod-shaped with smooth surface and the length and width if which are approximately 1.4 ± 0.2 and 0.6 ± 0.1 μm, respectively (Supplementary Figure S1a,b). The synthesized Fe_3O_4@*B. subtilis* SPMC maintain the bacilliform morphology of *B. subtilis* cells, but with much rougher surfaces, indicating successful coating of Fe_3O_4 magnetic nanoparticles (Figure 1b). The rougher surfaces may be beneficial for the photocatalytic ability by providing a higher specific surface area (Supplementary Figure S2). Moreover, the slight increase in diameter (length = 1.45 ± 0.5 μm; width = 0.65 ± 0.3 μm (Supplementary Figure S1c,d)) in comparison with *B. subtilis* cells provides assertive evidence that the Fe_3O_4 MNPs are attached onto the surfaces of *B. subtilis*. Furthermore, the magnification image (the insert image in Figure 1b) shows that some residual bare area on the surface of *B. subtilis* still remain, which might be used as adsorption sites for pollutants. The elemental composition of the prepared samples was studied by Energy Dispersive X-ray Spectroscopy (EDX) analysis. Comparing Figure 2c,d, the detection of Fe element confirmed the anchor of Fe_3O_4 MNPs onyto the *B. subtilis* surfaces. Simultaneously, two-dimensional X-ray mapping of Fe_3O_4@*B. subtilis* (Supplementary Figure S3) clearly shows the dispersions of C, O, and Fe elements on the microorganism surfaces.

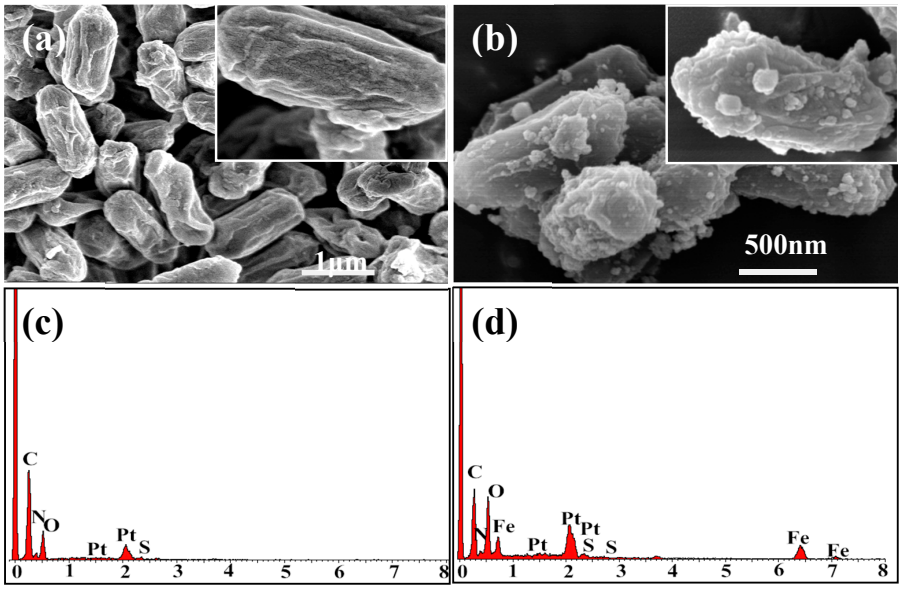

Figure 1. (**a**,**b**) Scanning electron microscope (SEM) images and (**c**,**d**) EDX spectra for *B. subtilis* and Fe_3O_4@*B. subtilis*.

The crystallographic structure of the as-obtained products was determined by XRD analysis (Figure 2a). The broad peak around 2θ = 20° shows that *B. subtilis* is amorphous (black curve) [13,15]. All the diffraction peaks of Fe_3O_4 MNPs (blue curve) could be readily indexed as face-centered cubic structured Fe_3O_4, which coincides well with the standard data (JCPDS card No. 19-0629) [17]. It is noted that the diffraction peaks corresponding to Fe_3O_4 are also presented in the XRD pattern of Fe_3O_4@*B. subtilis* SPMC (red curve), confirming the successful coating of Fe_3O_4 nanoparticles onto the surfaces of *B. subtilis*.

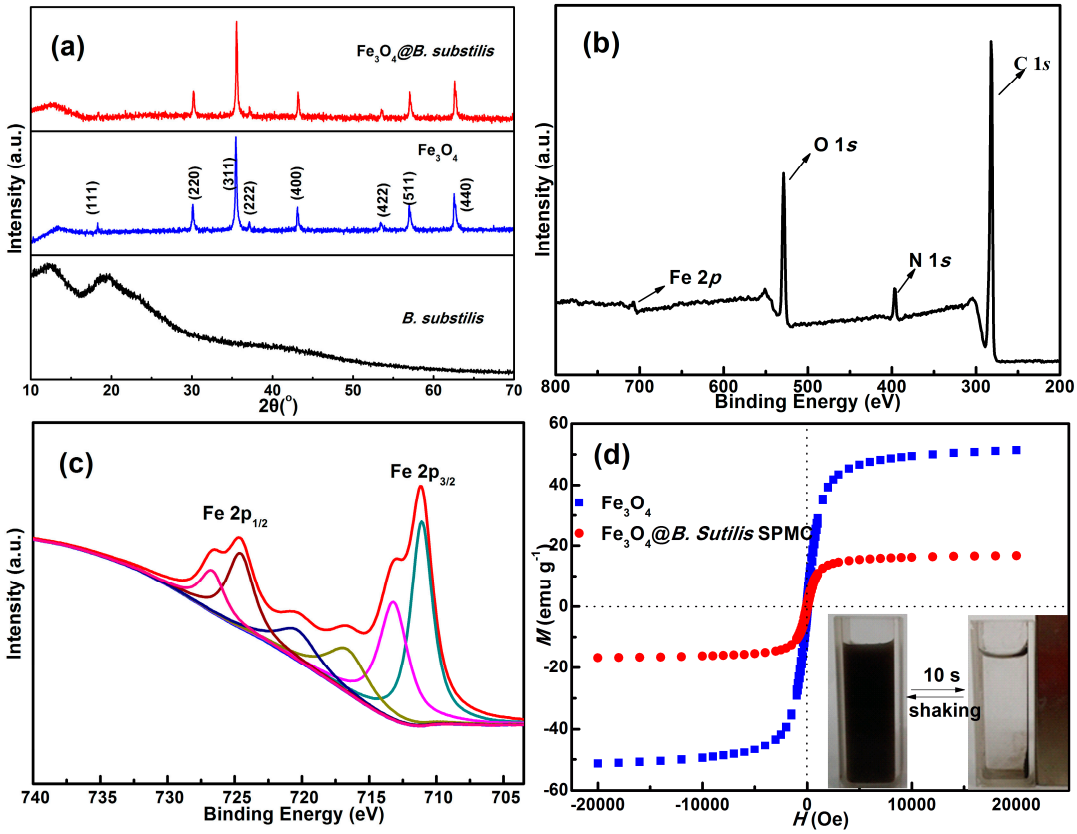

Figure 2. (**a**) XRD patterns of *B. subtilis*, Fe_3O_4, and Fe_3O_4@*B. subtilis* SPMC; (**b**) wide scan XPS spectra and (**c**) high resolution Fe 2p spectra of Fe_3O_4@*B. subtilis* SPMC; (**d**) hysteresis loops of Fe_3O_4 and Fe_3O_4@*B. subtilis* SPMC and its the separation-redispersion process (insert image).

XPS measurement was employed to characterize the Fe oxidation state in Fe_3O_4@*B. subtilis* SPMC. The photoelectron lines at binding energies of about 282.1, 397.0, 531.0, and 711.2 eV are attributed to C 1s, N 1s, O 1s, and Fe 2p, respectively (Figure 2b) [18]. In Figure 2c, two main peaks with satellite peaks between 705.0 and 735.0 eV are resolved at 710.9 eV and 724.5 eV, which are assigned to Fe $2p_{1/2}$ and Fe $2p_{3/2}$, respectively, and are consistent with the standard Fe_3O_4 XPS spectrum [18,19]. In addition, the elemental concentration of C, N, O and Fe in atomic % calculated according to relative sensitivity factors (RSFs) and spectra intensities were 69.02%, 4.0%, 22.87%, and 4.13%, respectively.

The magnetically controllable aggregation behavior of Fe_3O_4@*B. subtilis* was investigated by VSM study. Figure 2d shows the magnetic hysteresis loops of Fe_3O_4 and Fe_3O_4@*B. subtilis* SPMC with an extra magnetic field of 20,000 Oe at 300 K. The negligible coercivity (Hc) of hysteresis loop (71.1 Oe) and consequently no remanence (Mr, 1.23 emu/g) indicate the superparamagnetic nature of the Fe_3O_4@*B. subtilis* SPMC [20], exhibiting excellent redispersion stability (Figure 2d, inset). The saturation magnetization of the Fe_3O_4@*B. subtilis* SPMC (16.8 emu g^{-1}) is lower than the pristine Fe_3O_4 because of the non-magnetic properties of *B. subtilis*. In their homogeneous dispersion, Fe_3O_4@*B. subtilis* SPMC show quick movement under the extra magnetic field and re-disperse quickly with a slight shake

after removing the magnetic field, suggesting the prepared Fe_3O_4@*B. subtilis* SPMC presents excellent magnetic responsivity and redispersibility [21].

2.2. Fenton-Like Catalytic Degradation of Doxycycline

To test the catalytic performance of the as-prepared Fe_3O_4@*B. subtilis* SPMC, Fenton-like reactions were conducted for DC degradation. Comparable dosages of Fe_3O_4@*B. subtilis*, *B. subtilis* and Fe_3O_4 were used. Direct oxidation (blank) by H_2O_2 without any particles was also performed as a reference. Solution pH values were not controlled during the degradation process because they decreased very slightly ($\Delta pH < 0.5$).

As depicted in Figure 3a, direct oxidation of DC molecules (blank) by H_2O_2 is negligible. *B. subtilis* shows very low removal rate for DC within 30 min. When the Fe_3O_4@*B. subtilis* SPMC were used as catalyst, DC was nearly degraded completely in 30 min, showing a superior high catalytic activity in the Fenton-like system. Contrastively, under the same reaction condition, only 68.5% of DC was degraded by the as-synthesized Fe_3O_4 MNPs. The pseudo-first-order reaction was used to describe the kinetics of these catalytic reactions, and the rate constants k for DC degradation are calculated according to the regression curves of $-\ln(C/C_0)$ vs. time (t) (Figure 3b). The Fe_3O_4@*B. subtilis* SPMC shows a highest k value of 0.129 min^{-1}, followed by Fe_3O_4 (0.0374 min^{-1}) and *B. subtilis* (0.00222 min^{-1}), indicating the faster catalytic degradation kinetics and stronger catalytic ability of Fe_3O_4@*B. subtilis* SPMC.

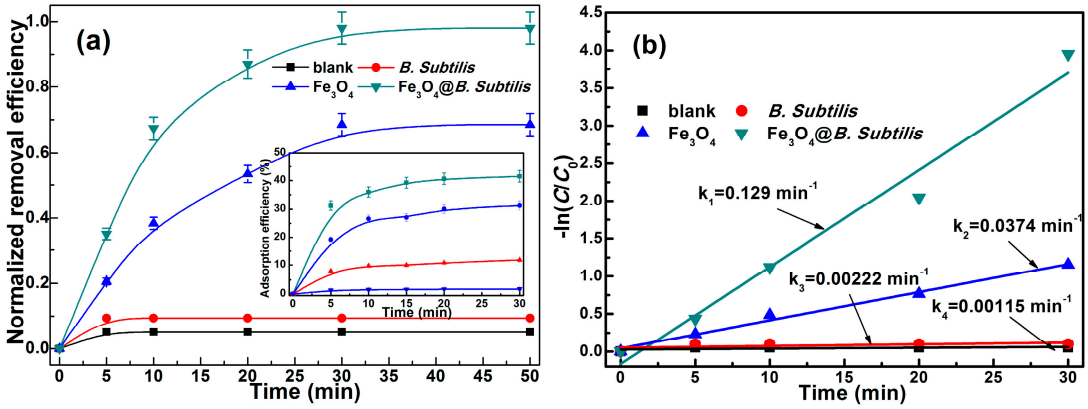

Figure 3. (**a**) Degradation and adsorptive (inset) performances for DC over as-prepared samples (*B. subtilis*, 0.35 g L^{-1}; Fe_3O_4, 0.125 g L^{-1}; Fe_3O_4@*B. subtilis* SPMC, 0.5 g L^{-1}): initial concentration of DC, 25 mg L^{-1}; H_2O_2 (20 mmol), room temperature, agitation speed 150 rpm; (**b**) $-\ln(C/C_0)$ as a function of time for DC degradation.

The enhanced catalytic activity of Fe_3O_4@*B. subtilis* SPMC compared to pristine *B. subtilis* and Fe_3O_4 MNPs can be attributed to the synergistic effect between adsorption by the *B. subtilis* bodies and Fenton-like oxidation by the Fe_3O_4 particles. The isoelectric point of Fe_3O_4@*B. subtilis* SPMC was determined to be 4.1 according to the zeta potentials curves (Supplementary Figure S4). Thus, the negative charge of Fe_3O_4@*B. subtilis* SPMC surfaces can absorb cationic form of DC via electrostatic interaction at neutral pH, resulting in a higher reactant concentration around the composite surfaces. In turn, the adsorption sites on the *B. subtilis* surface can be refreshed because of the decomposition of the DC molecules by $Fe^{2+}/Fe^{3+}/H_2O_2$ Fenton-like system.

2.3. Effect of H_2O_2 Dosage on Degradation of DC

The degradation efficiency of DC increased with increasing H_2O_2 dosage from 5.0 to 20.0 mmol, and then slightly decreased beyond 20.0 mmol (Figure 4a). The decreased DC removal under higher H_2O_2 dosage may be because that excessive H_2O_2 can induce OH· radicals scavenging effect (HO· + H_2O_2 → HOO· + H_2O) [15,22]. It is noteworthy that the generation of another radical HOO·,

whose oxidation ability is much lower than that of the HO· radicals, shows much less contribution to DC degradation [23]. Therefore, the initial H_2O_2 dosage was selected as 20.0 mmol to achieve the highest removal of DC in the present work.

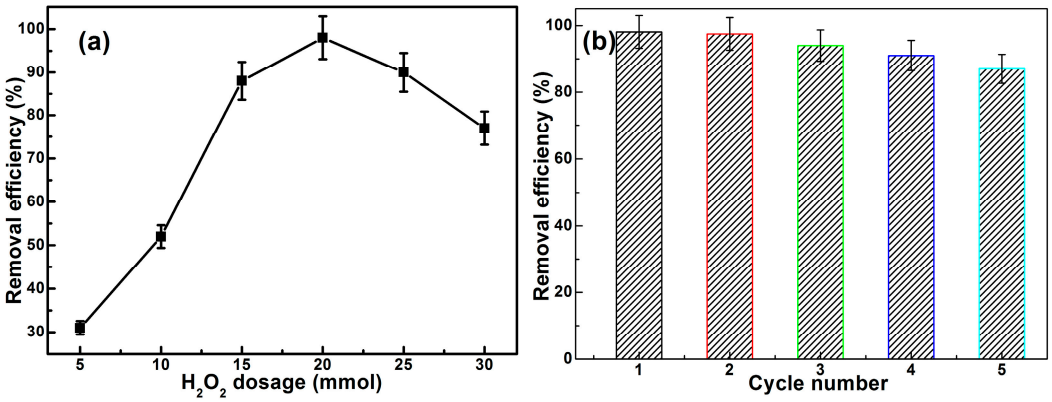

Figure 4. (**a**) Effect of H_2O_2 dosage on removal efficiency of DC by Fe_3O_4@*B. subtilis* SPMC (catalyst dosage 0.5 g L^{-1}, initial concentration of DC 25 mg L^{-1}, netural pH, room temperature); (**b**) The cyclic utilization of Fe_3O_4@*B. subtilis* SPMC for degradating DC (catalyst dosage 0.5 g L^{-1}, initial concentration of DC 25 mg L^{-1}, H_2O_2 20 mmol, netural pH, room temperature).

2.4. Iron Ion Leaching

To exclude the possibility that the observed catalytic activity of Fe_3O_4@*B. subtilis* SPMC in Fenton-like system is caused by the leaching ions, similar batch reactors with solutions (100 mL) containing Fe_3O_4@*B. subtilis* SPMC (0.5 g L^{-1}) at a neutral pH were mechanically stirred for 30 min at room temperature. Then, the Fe_3O_4@*B. subtilis* SPMC were removed by centrifugation to obtain leaching solution. 0.1 mL of the above supernatant was diluted with 4.9 mL HNO_3 (5%) to analyze the dissolved ions with ICP-MS. The result shows a Fe ions concentration of 0.612 ppm, which correspond to about 0.68% of the total Fe content in Fe_3O_4@*B. subtilis* SPMC. The remaining part of the leaching solution was employed to the homogeneous Fenton-like degradation of DC, and was initiated by the addition of fresh H_2O_2. By adding 2.5 mg DC and 20 mmol H_2O_2, only 7.5% of DC was removed within 30 min, which was much less than the removal of 98.1% in the Fe_3O_4@*B. subtilis* SPMC-H_2O_2 Fenton-like system at neutral pH (Figure 4a). Since the homogeneous degradation is negligible, the DC degradation at neutral pH mainly originates from the heterogeneous Fe_3O_4@*B. subtilis* SPMC-H_2O_2 Fenton-like system instead of the leached ions.

2.5. Stability and Reusability

The reusability and stability of Fe_3O_4@*B. subtilis* SPMC was evaluated by successive batches of DC degradation. After each run, Fe_3O_4@*B. subtilis* SPMC was re-collected, rinsed with DI water, and tested again. Fe_3O_4@*B. subtilis* SPMC can be reused for at least five consecutive runs, and the reused ones nearly retained the catalytic activity of the fresh catalyst (Figure 4b). The reusability of Fe_3O_4 was not investigated in this work because of two reasons: (1) the removal efficiency of DC, used for evaluation of reusability of Fe_3O_4@*B. subtilis* in Figure 4b, can be attributed the synergistic effect of adsorption by *B. subtilis* support and degradation by generated radicals, which is more complicated than bare Fe_3O_4; (2) Fe_3O_4 MNPs may present higher removal efficiency of DC after six cycles than that of Fe_3O_4@*B. subtilis* because they may leach much more iron ions for involving the Fenton-like process. However, in turn, more leaching ions means worse stability. Therefore, few publications have reported on the comparison between the repeatability of Fe_3O_4 and Fe_3O_4@support.

The good chemical stability of Fe_3O_4@*B. subtilis* SPMC was further confirmed by conducting XRD and XPS measurements after reaction. No considerable changes in XRD patterns (Figure 5a) were

observed after being reused for five cycles, indicating the stable chemical and crystalline structure of the Fe_3O_4@*B. subtilis* SPMC. XPS measurement (Figure 5b) demonstrates that the at % of C, N, O, and Fe are almost the same as those before reaction. These results indicate that Fe_3O_4@*B. subtilis* SPMC are durable and can be reused without great loss of catalytic activity in a long term Fenton-like reaction system at a neutral pH.

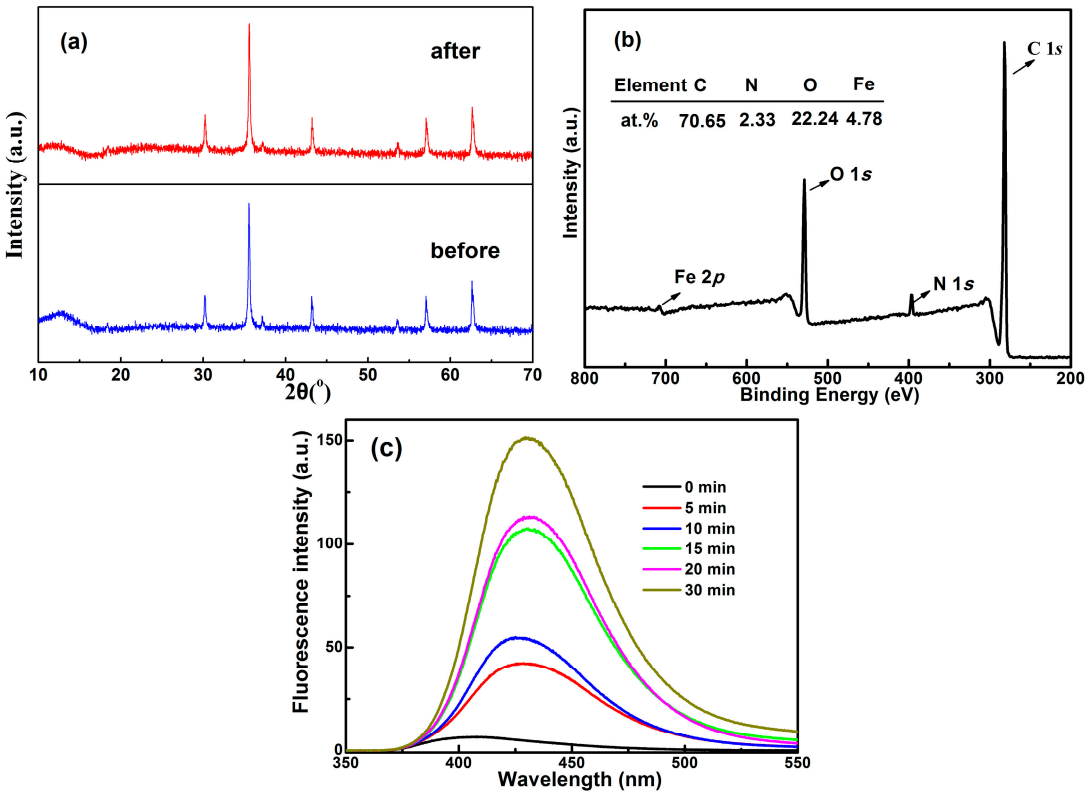

Figure 5. (**a**) XRD patterns of Fe_3O_4@*B. subtilis* SPMC before and after Fenton-like reaction; (**b**) wide scan XPS spectra of Fe_3O_4@*B. subtilis* SPMC after Fenton-like reaction; (**c**) Fluorescence spectral changes observed during Fenton-like process with Fe_3O_4@*B. subtilis* SPMC suspended in a 5×10^{-4} M basic solution of TA (λ_{exc} = 315 nm).

2.6. Degradation Mechanism

The dramatic Fenton-like catalytic activity of the as synthesized Fe_3O_4@*B. subtilis* SPMC motivated us to further investigate the mechanism of the Fenton-like degradation process. Although the Fenton-like reaction mechanism has not been fully understood, it is generally accepted that a series of reactive radical species (RRS)—such as HOO·, hydroxyl radical (OH·), superoxide radical ($O_2\cdot^-$), or singlet oxygen ($^1O_2$)—are supposed to be involved in the Fenton-like process [24–26]. However, which one plays the most important role in the Fenton-like process is still unclear, and is quite different from various systems. Luo et al. suggested that OH· radicals make a major contribution in the Fenton-like degradation of organic dyes at weak acidic conditions [27]. Li and co-workers demonstrated that the singlet oxygen $^1O_2$ produced from HOO· and HO· directly participates in the degradation of organic pollutants [25]. Therefore, on the basis of all the information obtained above and observations in the literatures [28–30], we propose that the mechanism of the H_2O_2 activation by Fe_3O_4@*B. subtilis* SPMC under neutral condition may involve the initial formation of complex intermediates between $\equiv Fe^{II}$, $\equiv Fe^{III}$, and H_2O_2, being marked as $H_2O_2 \equiv Fe^{II}$ Equation (1) and $H_2O_2 \equiv Fe^{III}$ Equation (2), where $\equiv Fe^{II}$ and $\equiv Fe^{III}$ stands for Fe(II) and Fe(III) sites on the surface of Fe_3O_4@*B. subtilis* SPMC. The intermediate $H_2O_2 \equiv Fe^{III}$ can convert to $\equiv Fe^{II}$ species and $HO_2\cdot$ (Equation (3). The generated $HO_2\cdot$ can further react with $\equiv Fe^{III}$ to produce $\equiv Fe^{II}$ species and O_2

Equation (4), giving an explanation of those bubbles generated in the reaction process. All the formed $\equiv Fe^{II}$ species Equations (3) and (4) and the initially generated $\equiv Fe^{II}$ species Equation (1) activate H_2O_2 to generate hydroxyl radicals HO· Equation (5), which is a very strong oxidative radical to degrade DC molecules Equation (6).

$$H_2O_2 + \equiv Fe^{II} \rightarrow H_2O_2 \equiv Fe^{II} \quad (1)$$

$$H_2O_2 + \equiv Fe^{III} \rightarrow H_2O_2 \equiv Fe^{III} \quad (2)$$

$$\equiv Fe^{III} + H_2O_2 \rightarrow \equiv Fe^{II} + HO_2\cdot + H^+ \quad (3)$$

$$\equiv Fe^{III} + HO_2 \rightarrow \equiv Fe^{II} + O_2 + H^+ \quad (4)$$

$$H_2O_2 + \equiv Fe^{II} \rightarrow \equiv Fe^{III} + HO\cdot + OH^- \quad (5)$$

$$HO\cdot + DC \rightarrow CO_2 + H_2O \quad (6)$$

Based on our hypothesis, HO· radicals make a great contribution to DC degradation by Fe_3O_4@*B. subtilis* SPMC. Thus, the formation of HO· was confirmed by the PL spectra using terephthalic acid (TA) as a probe molecule (Supplementary Figure S5). Figure 5 shows the fluorescence spectral changes observed during Fenton-like process with Fe_3O_4@*B. subtilis* suspended in a basic TA solution. As can be seen, with reaction time prolongs the PL intensity of 2-hydroxy terephthalic acid around 428 nm gradually increased, demonstrating the production of the hydroxyl radicals. Therefore, we can conclude that the enhanced degradation performance of DC by Fe_3O_4@*B. subtilis* under neutral pH can be due to the synergistic effect between the excellent adsorption ability and hydroxyl radicals generated from Fenton-like activation of H_2O_2 by Fe_3O_4@*B. subtilis* SPMC.

3. Experimental

3.1. Materials

B. subtilis powder was purchased from Guangzhou lvhui biological Company. All chemical reagents including $FeCl_3 \cdot 6H_2O$, $N_2H_4 \cdot H_2O$, CH_2O, H_2SO_4, and Doxycyline were purchased from Sigma-Aldrich (Sigma-Aldrich, St. Louis, MO, USA) and used directly without further purification. The chemical structure of doxycyline is presented in Figure 6. Absolute ethanol and double-distilled water were used through this work.

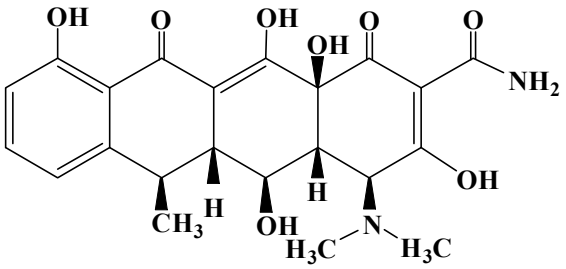

Figure 6. Chemical structure of Doxycyline.

3.2. Synthesis of Fe_3O_4 MNPs

Fe_3O_4 MNPs were synthesized through a hydrothermal method using $FeCl_3 \cdot 6H_2O$ as a single iron source [31]. Specifically, 1.20 g of $FeCl_3 \cdot 6H_2O$ was placed in a dry beaker, and then 5 mL of $N_2H_4 \cdot H_2O$ was added into the beaker dropwise with continuous stirring. After that, 2 mL of CH_2O and 33 mL deionized water were added into the baker, stirred for 10 min, and then the mixture was transferred to a 50 mL Teflon-lined stainless-steel autoclave and heated at 120 °C for 5 h. After cooling down, the black precipitate was collected with a magnet and washed with water and absolute ethanol for three times and then dried at 80 °C for 10 h.

3.3. Preparation of Fe_3O_4@B. subtilis Superparamagnetic Composite (SPMC)

Fe_3O_4@*B. subtilis* SPMC were fabricated based on an electrostatic attraction method (Supplementary Figure S6). Typically, dried magnetic Fe_3O_4 MNPs and 1.0 g of *B. subtilis* dry cell powder were dispersed in 100 mL of distilled water separately and the pH values was adjusted to 5.0 by adding 1 M H_2SO_4. The isoelectric points of Fe_3O_4 MNPs and *B. subtilis* were determined to be pH 2.2 and 6.6, respectively. Therefore, according to the zeta potential-pH curve (Supplementary Figure S4), at an experimental pH of 5.0, *B. subtilis* is negatively charged and Fe_3O_4 MNP is positively charged. Next, the two suspensions were sonicated for 20 min to facilitate deaggregation and then centrifuged. After that, the Fe_3O_4 MNPs and *B. subtilis* were re-dispersed in 100 mL distilled water separately and mixed under continuous mechanical stirring for 1 h at room temperature. The mixture was then left for 3.0 h at room temperature to form the Fe_3O_4@*B. subtilis* SPMC. The resulting particles were centrifuged, washed by ethanol and water for three times. The actual Fe content (18%, i.e., Fe_3O_4 content of 25%) in Fe_3O_4@*B. subtilis* SPMC was detected using ICP-MS. For the ICP-MS measurements, 10 mg Fe_3O_4@*B. subtilis* SPMC were first dissolved with 5 mL 5% concentrated HNO_3, and then diluted 50 times using HNO_3 (5%).

3.4. Characterizations

Scanning electron microscopy (SEM) images were recorded using a microscope (6300F, JEOL Ltd., Tokyo, Japan). The elemental composition was carried out by energy dispersive spectroscopy (EDX) analysis and energy dispersive X-ray (EDX) mapping. XRD patterns were acquired over a diffraction angle range (2θ) 5–80° using an X'Pert X-ray diffraction spectrometer with a Cu Kα X-ray source (MiniFlex 600, Rigaku, Tokyo, Japan). XPS spectra were obtained on an electron spectrometer (ESCALab220i-XL, VG Scientific, Waltham, MA, USA) using 300 W Al-Ka radiation. Magnetization measurements at room temperature were obtained using a vibrating sample magnetometer (Lake Shore Cryotronics, Inc., Carson, CA, USA).

3.5. Catalytic Tests

The catalytic performance of Fe_3O_4@*B. subtilis* SPMC was tested by the degradation of DC in semi-batch operation mode at neutral pH 0.05 g catalysts were dispersed into 100 mL aqueous solution of DC (25 mg L^{-1}) at room temperature. The suspensions were mechanically stirred in dark for 30 min to achieve the adsorption/desorption equilibrium. The DC concentrations after equilibration were measured and taken as the initial concentration (C_0). Then, the degradation reaction was initiated by the addition of H_2O_2 under mechanical stirring conditions at room temperature. At regular time intervals, about 5 mL of solution were taken out and immediately centrifuged at 10,000 rpm for 3 min, and the supernatant was determined by using a UV–vis spectrophotometer. Each experiment was conducted in triplicate.

3.6. Detection of Radical Species

Terephthalic acid (TA) was used to detect OH·. Briefly, 0.1 g Fe_3O_4@*B. subtilis* SPMC was dispersed in a 100 mL of the TA (5×10^{-4} mol L^{-1}) aqueous with an addition of 20.0 mmol H_2O_2 at room temperature and without any DC. The intensity of the PL signal at 428 nm was investigated on a fluorescence spectrophotometer (Shimadzu RF-5301PC, Tokyo, Japan) at an excitation wavelength of 315 nm.

4. Conclusions

In this study, novel superparamagnetic Fe_3O_4@*B. subtilis* Fenton-like catalyst was synthesized through a facile electrostatic attraction process. The obtained Fe_3O_4@*B. subtilis* exhibits significantly enhanced Fenton-like catalytic ability than pristine Fe_3O_4 and excellent recycling ability, reusability, and stability. The detailed doxycyline degradation mechanism was explored by employing

photoluminescence technology. The result clearly demonstrates that the synergistic effect of *Bacillus subtilis* adsorption and Fenton-like ability of Fe_3O_4 dominates the enhancement of Fenton-like catalytic efficiency of Fe_3O_4@*B. subtilis*.

Supplementary Materials: The following are available online at www.mdpi.com/2073-4344/7/11/349/s1, Figure S1: Size histogram of *B. subtilis* (a,b) and Fe_3O_4@ *B. subtilis* (c,d), Figure S2: N2 adsorption-desorption isotherm and pore size distribution (inset) of (a) the bare *B. subtilis* and (b) Fe_3O_4 MNP and (c) Fe_3O_4@*B. subtilis*, Figure S3: Selected zones of Fe_3O_4@*B. subtilis* SPMC (a) and corresponding X-ray mapping, for C (b), O (c), and Fe elements (d), Figure S4: Zeta potential of *B. subtilis*, Fe_3O_4 and Fe_3O_4@*B. subtilis* suspensions as a function of pH, Figure S5: Formation of hydroxyl products as the result of reaction between terephthalic acid (TA) and OH·, Figure S6: Schematic illustration of the synthesis process of Fe_3O_4@*B. subtilis*.

Acknowledgments: We thank Bo Bai and Weisheng Guan for their technical assistant and instruction through the experiments. This work was financially supported by the National Natural Science Foundation of China (21176031); Shanxi Provincial Natural Science Foundation of China (2015JM2071); the Fundamental Research Funds for the Central Universities (310829161004); and the Open Fund of Key Laboratory of Subsurface Hydrology and Ecological Effects in Arid Region, Ministry of Education of the People's Republic of China (No. 310829151140).

Author Contributions: Pei Zheng have made substantial contributions to experimental design and paper writing. Zhe Pan have made substantial contributions to data collection, analysis. Jun Zhang have revised it critically for important intellectual content.

Conflicts of Interest: The authors declare no conflict of interest.

References

1. He, C.; Wu, S.; Zhao, N.; Shi, C.; Liu, E.; Li, J. Carbon-encapsulated Fe_3O_4 nanoparticles as a high-rate lithium ion battery anode material. *ACS Nano* **2013**, *7*, 4459–4469. [CrossRef] [PubMed]
2. Yang, X.; Chen, W.; Huang, J.; Zhou, Y.; Zhu, Y.; Li, C. Rapid degradation of methylene blue in a novel heterogeneous Fe_3O_4@rGO@TiO_2-catalyzed photo-Fenton system. *Sci. Rep.* **2015**, *5*, 10632. [CrossRef] [PubMed]
3. Wang, F.; Pauletti, G.M.; Wang, J.; Zhang, J.; Ewing, R.C.; Wang, Y.; Shi, D. Dual surface-functionalized janus nanocomposites of polystyrene/Fe_3O_4@SiO_2 for simultaneous tumor cell targeting and stimulus-induced drug release. *Adv. Mater.* **2013**, *25*, 3485–3489. [CrossRef] [PubMed]
4. Xu, L.; Wang, J. Magnetic nanoscaled Fe_3O_4/CeO_2 composite as an efficient Fenton-like heterogeneous catalyst for degradation of 4-chlorophenol. *Environ. Sci. Technol.* **2012**, *46*, 10145–10153. [CrossRef] [PubMed]
5. Wei, Y.; Yin, G.; Ma, C.; Huang, Z.; Chen, X.; Liao, X.; Yao, Y.; Yin, H. Synthesis and cellular compatibility of biomineralized Fe_3O_4 nanoparticles in tumor cells targeting peptides. *Colloids Surf. B Biointerfaces* **2013**, *107*, 180–188. [CrossRef] [PubMed]
6. Zubir, N.A.; Yacou, C.; Motuzas, J.; Zhang, X.; da Costa, J.C.D. Structural and functional investigation of graphene oxide–Fe_3O_4 nanocomposites for the heterogeneous Fenton-like reaction. *Sci. Rep.* **2014**, *4*, 4594. [CrossRef] [PubMed]
7. Kuznetsova, E.; Savinov, E.; Vostrikova, L.; Parmon, V. Heterogeneous catalysis in the Fenton-type system FeZSM-5/H_2O_2. *Appl. Catal. B* **2004**, *51*, 165–170. [CrossRef]
8. Aravindhan, R.; Fathima, N.N.; Rao, J.R.; Nair, B.U. Wet oxidation of acid brown dye by hydrogen peroxide using heterogeneous catalyst Mn-salen-Y zeolite: A potential catalyst. *J. Hazard. Mater.* **2006**, *138*, 152–159. [CrossRef] [PubMed]
9. Yang, X.; Zhang, X.; Ma, Y.; Huang, Y.; Wang, Y.; Chen, Y. Superparamagnetic graphene oxide–Fe_3O_4 nanoparticles hybrid for controlled targeted drug carriers. *J. Mater. Chem.* **2009**, *19*, 2710–2714. [CrossRef]
10. Yu, L.; Yang, X.; Ye, Y.; Wang, D. Efficient removal of atrazine in water with a Fe_3O_4/MWCNTs nanocomposite as a heterogeneous Fenton-like catalyst. *RSC Adv.* **2015**, *5*, 46059–46066. [CrossRef]
11. Xu, H.-Y.; Shi, T.-N.; Zhao, H.; Jin, L.-G.; Wang, F.-C.; Wang, C.-Y.; Qi, S.-Y. Heterogeneous Fenton-like discoloration of methyl orange using Fe_3O_4/MWCNTs as catalyst: Process optimization by response surface methodology. *Front. Mater. Sci.* **2016**, *10*, 45–55. [CrossRef]
12. Li, X.; Huang, X.; Liu, D.; Wang, X.; Song, S.; Zhou, L.; Zhang, H. Synthesis of 3D hierarchical Fe_3O_4/graphene composites with high lithium storage capacity and for controlled drug delivery. *J. Phys. Chem. C* **2011**, *115*, 21567–21573. [CrossRef]

13. Yan, C.; Feng, D.; Jiang, Y.; An, X.; Ye, L.; Guan, W.; Bai, B. Bio-template Route for the Facile Fabrication of TiO_2@ *Bacillus subtilis* Composite Particles and Their Application for the Degradation of Rhodamine B. *Catal. Lett.* **2015**, *145*, 1301–1306. [CrossRef]
14. Filip, Z.; Herrmann, S.; Kubat, J. FT-IR spectroscopic characteristics of differently cultivated *Bacillus subtilis*. *Microbiol. Res.* **2004**, *159*, 257–262. [CrossRef] [PubMed]
15. Zheng, P.; Bai, B.; Guan, W.; Wang, H.; Suo, Y. Degradation of tetracycline hydrochloride by heterogeneous Fenton-like reaction using Fe@ *Bacillus subtilis*. *RSC Adv.* **2016**, *6*, 4101–4107. [CrossRef]
16. Ayla, A.; Çavuş, A.; Bulut, Y.; Baysal, Z.; Aytekin, Ç. Removal of methylene blue from aqueous solutions onto *Bacillus subtilis*: Determination of kinetic and equilibrium parameters. *Desalination Water Treat.* **2013**, *51*, 7596–7603. [CrossRef]
17. Liu, J.; Che, R.; Chen, H.; Zhang, F.; Xia, F.; Wu, Q.; Wang, M. Microwave absorption enhancement of multifunctional composite microspheres with spinel Fe_3O_4 cores and anatase TiO_2 shells. *Small* **2012**, *8*, 1214–1221. [CrossRef] [PubMed]
18. Kaboudin, B.; Mostafalu, R.; Yokomatsu, T. Fe_3O_4 nanoparticle-supported Cu (II)-β-cyclodextrin complex as a magnetically recoverable and reusable catalyst for the synthesis of symmetrical biaryls and 1, 2, 3-triazoles from aryl boronic acids. *Green Chem.* **2013**, *15*, 2266–2274. [CrossRef]
19. Mahdavi, M.; Namvar, F.; Ahmad, M.B.; Mohamad, R. Green biosynthesis and characterization of magnetic iron oxide (Fe_3O_4) nanoparticles using seaweed (*Sargassum muticum*) aqueous extract. *Molecules* **2013**, *18*, 5954–5964. [CrossRef] [PubMed]
20. Hassan, M.S.; Amna, T.; Yang, O.-B.; Kim, H.-C.; Khil, M.-S. TiO_2 nanofibers doped with rare earth elements and their photocatalytic activity. *Ceram. Int.* **2012**, *38*, 5925–5930. [CrossRef]
21. Deng, Y.; Qi, D.; Deng, C.; Zhang, X.; Zhao, D. Superparamagnetic high-magnetization microspheres with an Fe_3O_4@ SiO_2 core and perpendicularly aligned mesoporous SiO_2 shell for removal of microcystins. *J. Am. Chem. Soc.* **2008**, *130*, 28–29. [CrossRef] [PubMed]
22. Tian, S.; Zhang, J.; Chen, J.; Kong, L.; Lu, J.; Ding, F.; Xiong, Y. $Fe_2(MoO_4)_3$ as an effective photo-Fenton-like catalyst for the degradation of anionic and cationic dyes in a wide pH range. *Ind. Eng. Chem. Res.* **2013**, *52*, 13333–13341. [CrossRef]
23. Bigda, R.J. Consider Fentons chemistry for wastewater treatment. *Chem. Eng. Prog.* **1995**, *91*, 62–66.
24. Coelho, J.V.; Guedes, M.S.; Prado, R.G.; Tronto, J.; Ardisson, J.D.; Pereira, M.C.; Oliveira, L.C. Effect of iron precursor on the Fenton-like activity of Fe_2O_3/mesoporous silica catalysts prepared under mild conditions. *Appl. Catal. B* **2014**, *144*, 792–799. [CrossRef]
25. Li, X.; Liu, J.; Rykov, A.I.; Han, H.; Jin, C.; Liu, X.; Wang, J. Excellent photo-Fenton catalysts of Fe–Co Prussian blue analogues and their reaction mechanism study. *Appl. Catal. B* **2015**, *179*, 196–205. [CrossRef]
26. Cleveland, V.; Bingham, J.-P.; Kan, E. Heterogeneous Fenton degradation of bisphenol A by carbon nanotube-supported Fe_3O_4. *Sep. Purif. Technol.* **2014**, *133*, 388–395. [CrossRef]
27. Luo, W.; Zhu, L.; Wang, N.; Tang, H.; Cao, M.; She, Y. Efficient removal of organic pollutants with magnetic nanoscaled $BiFeO_3$ as a reusable heterogeneous Fenton-like catalyst. *Environ. Sci. Technol.* **2010**, *44*, 1786–1791. [CrossRef] [PubMed]
28. Hu, X.; Liu, B.; Deng, Y.; Chen, H.; Luo, S.; Sun, C.; Yang, P.; Yang, S. Adsorption and heterogeneous Fenton degradation of 17α-methyltestosterone on nano Fe_3O_4/MWCNTs in aqueous solution. *Appl. Catal. B* **2011**, *107*, 274–283. [CrossRef]
29. Kwan, W.P.; Voelker, B.M. Rates of hydroxyl radical generation and organic compound oxidation in mineral-catalyzed Fenton-like systems. *Environ. Sci. Technol.* **2003**, *37*, 1150–1158. [CrossRef] [PubMed]
30. Yang, X.-J.; Xu, X.-M.; Xu, J.; Han, Y.-F. Iron oxychloride (FeOCl): An efficient Fenton-like catalyst for producing hydroxyl radicals in degradation of organic contaminants. *J. Am. Chem. Soc.* **2013**, *135*, 16058–16061. [CrossRef] [PubMed]
31. Song, R.; Bai, B.; Puma, G.L.; Wang, H.; Suo, Y. Biosorption of azo dyes by raspberry-like Fe_3O_4@ yeast magnetic microspheres and their efficient regeneration using heterogeneous Fenton-like catalytic processes over an up-flow packed reactor. *React. Kinet. Mech. Cat.* **2015**, *115*, 547–562. [CrossRef]